

# JAAS

Accepted Manuscript



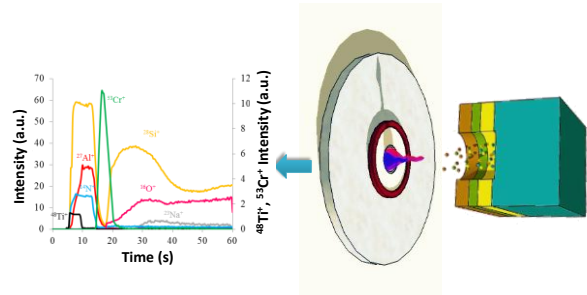
This is an *Accepted Manuscript*, which has been through the Royal Society of Chemistry peer review process and has been accepted for publication.

*Accepted Manuscripts* are published online shortly after acceptance, before technical editing, formatting and proof reading. Using this free service, authors can make their results available to the community, in citable form, before we publish the edited article. We will replace this *Accepted Manuscript* with the edited and formatted *Advance Article* as soon as it is available.

You can find more information about *Accepted Manuscripts* in the [Information for Authors](#).

Please note that technical editing may introduce minor changes to the text and/or graphics, which may alter content. The journal's standard [Terms & Conditions](#) and the [Ethical guidelines](#) still apply. In no event shall the Royal Society of Chemistry be held responsible for any errors or omissions in this *Accepted Manuscript* or any consequences arising from the use of any information it contains.

1  
2  
3  
4  
5  
6  
7  
8  
9  
10  
11  
12  
13  
14  
15  
16  
17  
18  
19  
20  
21  
22  
23  
24  
25  
26  
27  
28  
29  
30  
31  
32  
33  
34  
35  
36  
37  
38  
39  
40  
41  
42  
43



*The potential of rf-PGD-ToFMS for quantitative depth profiling analysis of thin layers on glasses has been investigated*

1  
2  
3  
4  
5  
6  
7  
8  
9  
10  
11  
12  
13  
14  
15  
16  
17  
18  
19  
20  
21  
22  
23  
24  
25  
26  
27  
28  
29  
30  
31  
32  
33  
34  
35  
36  
37  
38  
39  
40  
41  
42  
43  
44  
45  
46  
47  
48  
49  
50  
51  
52  
53  
54  
55  
56  
57  
58  
59  
60

**PULSED RADIOFREQUENCY GLOW DISCHARGE TIME OF  
FLIGHT MASS SPECTROMETRY FOR COATED GLASS  
ANALYSIS**

Marcos Bouza<sup>1</sup>, Rosario Pereiro<sup>1</sup>, Nerea Bordel<sup>2</sup>, Alfredo Sanz-Medel<sup>1</sup>,  
Beatriz Fernández<sup>1\*</sup>

<sup>1</sup>*Department of Physical and Analytical Chemistry, Faculty of Chemistry; University of  
Oviedo; Julian Clavería, 8; 33006 Oviedo, Spain*

<sup>2</sup>*Department of Physics, University of Oviedo, Spain*

\*Author to whom correspondence should be addressed

Corresponding author: fernandezbeatriz@uniovi.es

Tel: +34 985103512

**ABSTRACT**

The analytical potential of radiofrequency pulsed glow discharge time of flight mass spectrometry (rf-PGD-ToFMS) is investigated for quantitative depth profiling analysis of glasses and thin conductive and non-conductive layers on glasses. PGDs in combination with ToFMS can allow the reduction or even removal of spectral interferences by selecting a proper GD pulse interval. Thus, discrimination of potential polyatomic interferences for several analytes (e.g.,  $^{28}\text{Si}^+$ ,  $^{39}\text{K}^+$ ,  $^{44}\text{Ca}^+$ , and  $^{48}\text{Ti}^+$ ) were investigated by selecting appropriate time positions along the GD pulse profile. In this paper, the determination of compositional depth profiles of coated glasses was performed by resorting to a multi-matrix calibration procedure. For this purpose, conductive as well as non-conductive certified reference materials were employed to build the analytical calibration curves. Results show that rf-PGD-ToFMS allows us to discriminate the different layers of the samples and the nominal values for element concentrations and layer thicknesses were in agreements with experimental results obtained using the proposed quantification strategy. Moreover, the capabilities of rf-PGD-ToFMS to provide a full mass spectrum every 33  $\mu\text{s}$  enable the identification of unexpected elements which can be present as contaminants in very thin layers (e.g. Cd, Sn, Te and Sb).

**KEYWORDS:** Pulsed glow discharge; Time of flight mass spectrometry; Depth profiling; Glass determinations.

## 1. INTRODUCTION

Glow discharge coupled to optical-emission spectrometry (OES) has become a competitive tool for depth profiling of materials due to comparatively good depth resolution (in the nanometer scale), low matrix effects and high sample throughput (a few minutes per analysis)<sup>1</sup>. Direct current (dc) voltage has been traditionally used, but GDs can also be produced with radiofrequency (rf) energy. In this latter case, conducting and insulating samples can be directly analysed,<sup>2</sup> so expanding the applications field of GDs. Moreover, it has been shown how the application of power pulses to the GDs gives rise to a higher analytical sensitivity while reducing the thermal stress to the analysed solid sample (of special interest for the analysis of fragile and thermally unstable materials such as glasses).<sup>3</sup>

The coupling of GDs to mass spectrometry (MS) for depth profiling purposes has been less extended; however, it has aroused increasing interest.<sup>4</sup> In particular, coupling a rf-pulsed GD (PGD) with a time of flight mass spectrometer (ToFMS) offers today a very promising approach for the analysis of thin layers.<sup>5</sup> Among the significant advantages brought about by the combination of a PGD to a ToFMS, the possibility of reduction or even removal of some spectral interferences by selecting a proper pulse interval should be stressed.<sup>6-8</sup>

Rf-PGD-ToFMS offers interesting advantages as compared to conventional GD-OES, such as higher sensitivity for elemental determinations, full coverage of almost all the elements of the Periodic Table in a single run (highly valuable feature to detect unexpected elements and contaminants in layers), and isotopic measurement capabilities. Comparing to other mass spectrometric surface analysis techniques like SIMS, it is worth to highlight the lower matrix effects and fast analysis time typical of GD depth profiling. In recent years, rf-PGD-ToFMS has been successfully employed for varied applications, including the analysis of thermoelectric layers on Si wafers,<sup>9</sup> ultra-low energy implants,<sup>10</sup> fluorine-containing tantalum layers,<sup>11</sup> and even polymers,<sup>12</sup> among others. Depth analysis of coated glasses has already been attempted, but only qualitative depth profiling has been reported so far.<sup>13</sup>

Different approaches developed to obtain quantitative compositional depth profiling using GD-OES are based on the assumption that the “emission yield” (i.e. number of photons measured at the wavelength selected per sputtered atom of a given element) in GDs is essentially a matrix independent quantity.<sup>14</sup> In the case of GD-MS, for depth profiling of conducting matrices successful attempts have been carried out by

1  
2  
3 using a conceptually rather similar factor than emission yields: the so-called “absolute  
4 sensitive factors” ( $S_i$ ).<sup>15</sup> However, to our knowledge, quantification of coated insulator  
5 materials has not yet been investigated by GD-MS. This can be attributed to the fact that  
6 non-conductive samples (e.g. glasses) have high oxygen content which could affect the  
7 ionization mechanisms within the discharge.<sup>16</sup>  
8  
9

10 For all the above motivations, the quantitative elemental analysis and depth  
11 profiling of selected glasses has been undertaken here using rf-PGD-ToFMS as a highly  
12 appropriate analytical tool.  
13  
14  
15  
16

## 17 18 19 **2. EXPERIMENTAL**

### 20 **2.1. Instrumentation**

21 A rf-PGD-ToFMS prototype was used for the experiments. It has a rf-PGD bay  
22 unit (provided with a pulsed RF generator, matching box, RF-connector and a mounting  
23 system with a pneumatic piston to press the sample against the GD) supplied by Horiba  
24 Jobin Yvon (Longjumeau, France).<sup>13</sup> The rf-PGD source is coupled to an orthogonal  
25 time-of-flight mass spectrometer (TOFWERK, Switzerland) with a microchannel plate  
26 detector.<sup>17</sup> This coupling was performed with a 0.5 mm orifice diameter sampler and a  
27 1.0 mm orifice diameter skimmer, with a separation of 7 mm between them.  
28  
29  
30  
31  
32  
33

34 A GD chamber which in previous studies has been denoted as UNIOVI GD was  
35 used for this work.<sup>18</sup> The UNIOVI GD consists of a stainless steel disk of 45 mm  
36 diameter and 7 mm thickness allowing a short distance from the sample surface to the  
37 sampler cone (approximately 8.8 mm). The discharge gas was driven to the anode  
38 cylinder through eight concentric inner channels (located about 2 mm from the cathode  
39 surface) which constrain the GD plasma in a symmetric way. The cylindrical orifice of  
40 the anode restricts the “sputtering spot” to a well-defined circular area of 4 mm diameter  
41 on the sample surface. A ceramic piece located on the top of the source maintained the  
42 distance between anode and cathode at around 0.2 mm. Moreover, an o-ring is placed  
43 around the ceramic piece to prevent vacuum losses. To minimize risks of spectral  
44 interferences of polyatomics arising from air components, 3 min was waited once the  
45 sample was fixed, before igniting the GD.  
46  
47  
48  
49  
50  
51  
52  
53  
54  
55

56 The GD source can generate pulses with a pulse period from 0.1 ms up to 100  
57 ms and pulse widths from 50  $\mu$ s up to several milliseconds. The radiofrequency  
58 generator operates at 13.56 MHz. The power is supplied from the back side of the  
59 sample and a refrigerating disc is used to keep the samples at temperatures lower than  
60

1  
2  
3 6°C. In our case, 2 ms of pulse width and 4 ms of pulse period (250 Hz with 50% duty  
4 cycle) were selected for the measurements. The ToFMS was operated with an ion  
5 extraction rate of 1 extraction/33  $\mu$ s. Further details of this GD-MS instrument can be  
6 found in previous work.<sup>7</sup>  
7  
8  
9

## 10 11 12 **2.2. Standard Materials for Calibration and Samples**

13 Calibration with glasses by rf-PGD-ToFMS was performed using the materials  
14 collected in Table 1 (the selected glass standards are 6 mm thick). Reference material  
15 NIST 621 is from National Institute of Standards and Technology (Gaithersburg MD,  
16 USA) and the rest of reference materials are special silicate glasses for XRF monitoring  
17 from Brei $\ddot{t}$ l $\ddot{a}$ nder (Hamm, Germany). As can be seen, the glass standards collected in  
18 Table 1 covers a very wide elemental concentration interval. Additionally, for some  
19 other experiments it has been used the 4 mm thick NIST93A glass from National  
20 Institute of Standards and Technology (Gaithersburg MD, USA). On the other hand, 17  
21 bulk certified reference materials (CRMs) were also used for quantification of the thin  
22 conductive layers. Multiple matrices, including Fe, Ti, Al, and Ni, as well as wide  
23 ranges of analyte mass fractions were used in the calibration curves with conductive  
24 CRMs: elemental concentrations varied from few  $\mu$ g/g (ppm) up to high percentages  
25 (e.g. 99.4% Ti).  
26  
27  
28  
29  
30  
31  
32  
33  
34  
35  
36

37 Before the analysis by rf-PGD-ToFMS, conductive calibrating materials were  
38 polished using metallographic grinding papers (SiC: 220, 800 and 1200 grit) and then  
39 cleaned with ethanol to avoid contamination. For all the standards, the shape and depth  
40 of the craters were measured by mechanical profilometry (Perth-o-meter S5P,  
41 MahrPerthen, Germany). Two profile traces in different directions across the centre of  
42 each crater were measured in all cases. Sputtering rates ( $q_m$ ), evaluated as mass loss per  
43 unit time during the sputtering, were calculated by measuring the penetration depths per  
44 unit time and considering the crater diameter and material density.<sup>14</sup> The mean of three  
45 sputtered replicates was always used.  
46  
47  
48  
49  
50  
51  
52

53 The investigated coated glass samples (TL1 and TL2), provided by Saint Gobain  
54 Glass (Avilés, Spain), consisted on thin films on glass substrates with the following  
55 layer distribution: 27 nm  $\text{Si}_x\text{N}_y$ /12 nm Nb/20 nm  $\text{SiO}_2$ //6 mm glass (TL1) and 4 nm  
56 Ti/10 nm  $\text{Si}_x\text{N}_y$ /6 nm Cr/20 nm  $\text{SiO}_2$ //6 mm glass (TL2).  
57  
58  
59  
60

### 3. RESULTS AND DISCUSSION

Experimental conditions (300 Pa, 80 W rf forward power, 2 ms pulse width and 4 ms pulse period) were optimised and selected as a compromise between high sensitivity and good depth resolution.

#### 3.1. Interference Removal Studies

As expected, higher intensity analytical signals were obtained in the afterglow region of the GD pulse profile.<sup>7</sup> As above mentioned, PGDs in combination with ToFMS can allow the reduction or even removal of spectral interferences by selecting a proper GD pulse interval. Fig. 1 collects the observed afterglow pulse profiles of  $^{23}\text{Na}^+$ ,  $^{24}\text{Mg}^+$ ,  $^{27}\text{Al}^+$ ,  $^{28}\text{Si}^+$  and  $m/z$  40 (which should include the contribution of  $^{40}\text{Ca}^+$  and  $^{40}\text{Ar}^+$ ) in the analysis of D1 glass by rf-PGD-ToFMS. The time afterglow region selected for measurement of  $^{23}\text{Na}^+$ ,  $^{24}\text{Mg}^+$ ,  $^{27}\text{Al}^+$  and  $^{28}\text{Si}^+$  (interval between 2.25 and 2.4 ms) is marked in Fig. 1 with a dotted rectangle. This interval proved to provide maximum sensitivity while potential polyatomic interferences (typically appearing at the end of the afterglow) were minimized or avoided.

The ability of PGDs combined to ToFMS for discrimination between the analytes and their spectral interferences can be clearly seen when measuring silicon and titanium (both present on the layers of the coated samples). The Ti isotope of higher abundance is  $^{48}\text{Ti}$  (73.72%) but  $^{15}\text{N}^{16}\text{O}_2^+\text{H}$  and  $^{14}\text{N}^{16}\text{O}^{18}\text{O}$  polyatomic ions can be also found at this mass spectrum region. As an example, Fig. 2a shows the obtained mass spectra at  $m/z$  48 of  $^{48}\text{Ti}^+$  in a sample containing 6.9% N (JK 41-1N) for different time intervals at the afterglow region. Although the standard material used does not contain oxygen, a smaller peak appearing at higher mass (corresponding to  $^{15}\text{N}^{16}\text{O}_2^+\text{H}$  and/or  $^{14}\text{N}^{16}\text{O}^{18}\text{O}^+$ ) can be observed. Such interferences can arise from potential small air leaks in the system and their presence seems to be noticeably only when using for measurement either the final part of the afterglow (pulse profile region where recombination processes are more probable) or the complete afterglow. In order to avoid the potential presence of those polyatomic signals, the time interval between 2.25 and 2.4 ms was selected for  $^{48}\text{Ti}^+$  determinations. Regarding  $^{28}\text{Si}^+$ , previous experiments have shown that polyatomic interferences of  $^{12}\text{C}^{16}\text{O}^+$  and  $^{14}\text{N}_2^+$  can be overcome with the UNIOVI GD source configuration when measuring in the region of the afterglow maximum.<sup>18</sup> As shown in Fig. 2b, two different peaks corresponding to the analyte and the polyatomic

interferences can be clearly observed in the mass spectra at  $m/z$  28 when using for measurement the proper GD pulse interval.

In this work, particular attention has been paid to overcome potential interferences of two elements which have not been investigated earlier with our rf-PGD-ToFMS prototype: potassium and calcium. The isotope  $^{39}\text{K}$  has an abundance of 93.26% and its signal can overlap with  $^{38}\text{Ar}^1\text{H}$  (a mass resolution of 5690 is required to resolve them). Previous experiments using a PGD coupled to sector field MS showed that it was possible to temporally resolve the spectra of support-gas and sample ions.<sup>19</sup> Fig. 3 shows the pulse profiles obtained with our instrument under the selected operating conditions at  $m/z$  39 for the standard B1, which does not contain potassium, and the standard F1 with a  $\text{K}_2\text{O}$  concentration of 19.3%. Therefore, in the first case the pulse profile corresponds to  $^{38}\text{Ar}^1\text{H}^+$  polyatomic ion whereas in the second case corresponds to both  $^{38}\text{Ar}^1\text{H}^+$  and  $^{39}\text{K}^+$ . Additionally, Fig. 3 also collects the pulse profile at  $m/z$  37 obtained for the standard F1. In this case, such profile corresponds to  $^{36}\text{Ar}^1\text{H}^+$  polyatomic ion. Pulse profiles of  $^{38}\text{Ar}^1\text{H}^+$  in standard B1 and  $^{36}\text{Ar}^1\text{H}^+$  in standard F1 were similar so the different shape observed for  $m/z$  39 in the standard F1 can be attributed to the contribution of  $^{39}\text{K}^+$ . As can be seen, the discharge gas polyatomic signal ( $^{38}\text{Ar}^1\text{H}^+$ ) tends to decrease earlier than the  $^{39}\text{K}^+$  signal (dotted line at the pulse profile at  $m/z$  39); however, although it is not clearly seen on the plot, a small signal for  $^{38}\text{Ar}^1\text{H}^+$  was observed along the whole profile, thus limiting the analysis of very low potassium concentrations. Therefore, to keep a compromise between high  $^{39}\text{K}^+$  intensity signals for lower potassium concentrations while overcoming the  $^{38}\text{Ar}^1\text{H}^+$  polyatomic interference, a 33  $\mu\text{s}$  interval at 2.7 ms after the pulse ignition was selected for data treatment and a mathematical correction approach was investigated for eliminate gas polyatomic signal. The correction approach consisted on measuring for each standard the signal intensity for  $^{36}\text{Ar}^1\text{H}^+$ , correcting it by the isotopic ratio ( $^{38}\text{Ar}^+ / ^{36}\text{Ar}^+$ ) in order to obtain the theoretical  $^{38}\text{Ar}^1\text{H}^+$  intensity, and then subtracting this value from the signal intensity measured at  $m/z$  39 for standards containing potassium.

In the case of calcium, the natural isotopes are:  $^{40}\text{Ca}$  (96.94%),  $^{42}\text{Ca}$  (0.647%),  $^{43}\text{Ca}$  (0.135%),  $^{44}\text{Ca}$  (2.09%),  $^{46}\text{Ca}$  (0.004%) and  $^{48}\text{Ca}$  (0.19%). Unfortunately, the mass resolution required to separate  $^{40}\text{Ca}$  and  $^{40}\text{Ar}$  exceeds 190 000. It has been previously described that discrimination against isobaric interferences arising from the discharge gas could be possible by selecting an appropriate time regime within the afterglow.<sup>20</sup> As collected in Fig.1, the afterglow at  $m/z$  40 ( $^{40}\text{Ar}^+$  and  $^{40}\text{Ca}^+$ ) falls down earlier than for

1  
2  
3 most sputtered analytes. Unfortunately, the smaller signals for the pulse profile of  
4  $^{40}\text{Ca}^+$  are rather hidden by the high signal coming from  $^{40}\text{Ar}^+$ , under our selected  
5 operating conditions. A possibility could be to measure the  $^{40}\text{Ca}$  isotope at the latter part  
6 of the afterglow (e.g. at 2.75 ms) but in this case the contribution of  $^{40}\text{Ar}^+$  to  $m/z$  40 is  
7 still significant.  
8  
9

10  
11  
12 Considering the use of alternative Ca isotopes as 42 and 43 masses, both were  
13 hidden by the  $^{40}\text{Ar}^1\text{H}^+$  tail, while  $^{46}\text{Ca}$  and  $^{48}\text{Ca}$  are present in a very low abundance. For  
14 such reasons, we have paid attention to the detection of  $^{44}\text{Ca}$ , even if this Ca isotope can  
15 be interfered by  $^{12}\text{C}^{16}\text{O}_2^+$  and  $^{28}\text{Si}^{16}\text{O}^+$  polyatomic ions. This option was further studied  
16 using three different samples: the NIST 621 glass (10.7% Ca, 72.13% Si), the NIST  
17 93A glass (0.01% Ca, 80.8% Si) and also a conductive 151X-FCA4 stainless steel (0%  
18 Ca, 0.01% Si). Considering previous experiments carried out in our group,<sup>8</sup> we  
19 investigated the prepeak region for  $^{44}\text{Ca}$  measurements as well (measurement in such  
20 time region may keep polyatomic interferences at a minimum). In our case, we tried  
21 here to measure at 0.15 ms after pulse start. Fig. 4 shows the observed mass spectrum  
22 for  $m/z$  44 (Fig. 4a) and  $m/z$  45 (Fig. 4b). As can be seen in Fig. 4a, although the  
23 standard NIST 93A has a rather low Ca concentration, a considerable signal  
24 corresponding to  $^{12}\text{C}^{16}\text{O}_2^+$  and  $^{28}\text{Si}^{16}\text{O}^+$  polyatomic interferences is observed at  $m/z$  44  
25 even at the prepeak region. The signal measured at  $m/z$  45 (Fig. 4b) is due to  $^{29}\text{Si}^{16}\text{O}^+$ ,  
26 therefore applying a mathematical correction based on the natural isotopic abundances  
27 of  $^{28}\text{Si}$  (92.22%) and  $^{29}\text{Si}$  (4.69%), such signal appearing at  $m/z$  45 can be used to  
28 subtract the contribution of  $^{28}\text{Si}^{16}\text{O}^+$  at  $m/z$  44. Concerning  $^{12}\text{C}^{16}\text{O}_2^+$  interference, the  
29 standard 151X-FCA4, which does not contain calcium and just a negligible  
30 concentration of Si, was also measured. As shown in Fig. 4a, the small peak observed at  
31  $m/z$  44 should mostly correspond to the  $^{12}\text{C}^{16}\text{O}_2^+$  polyatomic ion and thus it could be  
32 stated that the contribution of such polyatomic interference to  $m/z$  44 in the prepeak  
33 region is almost negligible. In other words, accurate measurement of  $^{44}\text{Ca}$  isotope using  
34 PGD-ToFMS is difficult due to the presence of two types of possible polyatomic  
35 interferences. However, as it is collected in next section, such interferences could be  
36 corrected to obtain calibration curves for Ca determinations in glasses.  
37  
38  
39  
40  
41  
42  
43  
44  
45  
46  
47  
48  
49  
50  
51  
52  
53  
54  
55  
56  
57

### 58 3.2. Glass calibration

59 The absolute sensitive factors (S) represent the ratio between the number of  
60 particles of a given sputtered isotope (species i) measured at the detector and the

number of particles of these species that are released from the solid surface. As in OES,<sup>14</sup> it could be assumed at a first approximation that  $S_i$  does not depend on the sample matrix. This means that the ion signal of the isotope measured of the corresponding analyte should be proportional to the sputtered mass of the element if operation parameters are kept constant. The absolute sensitive factors are given by the following equation:

$$S_i = I_i^+ / (q_m \cdot C_i) \quad (1)$$

where  $I_i^+$  is the intensity of the isotope measured of analyte  $i$ ,  $q_m$  is the sputtering rate of the material (in mass per unit area per second) and  $C_i$  is the concentration of analyte  $i$ .

Fig. 5 collects plots of ion signal intensity *versus* the product of “sample sputtering rate” and “the concentration of the corresponding element” for aluminium, oxygen, silicon, potassium and sodium using the 6 mm thick glass calibrating materials collected in Table 1 measured by rf-PGD-ToFMS. It is worth mentioning that standard E1 was not used for calibration purposes but was used to check the validity of the calibration curves using it as an external sample. “To determine sputtering rates (main error source in GD quantification procedures), three replicates of the standards were subjected to 1600 s of sputtering and results are collected in Table 1; as it is collected in Table 1, the relative standard deviations are less than 10%. It is interesting to note that analytical signals remained stable and potential problems related with sample breaking due to possible overheating were not observed along such rather long sputtering times. For signal intensity measurement it has been selected the pulse interval between 2.25 and 2.4 ms for all the analytes, except potassium (33  $\mu$ s interval at 2.7 ms after the pulse ignition). As can be seen in Fig. 5, calibration plots showed a good linear correlation for all the elements. Regarding oxygen, its concentration in each standard was calculated by subtracting from 100% the concentrations of the other elemental components. Although the interval of concentrations measured for oxygen could be considered as comparatively small, it covers by far typical concentrations of oxygen in glass matrices.

In the case of calcium, Fig. 6 collects calibration curves obtained by rf-PGD-ToFMS for  $m/z$  44. As previously mentioned, to determine calcium in a precise and accurate way we investigated the  $^{44}\text{Ca}$  isotope applying a mathematical correction strategy to remove the possible polyatomic interferences (please note that in this case calibration graphs were plotted once the contribution from  $^{28}\text{Si}^{16}\text{O}^+$  was removed by considering the  $^{29}\text{Si}/^{28}\text{Si}$  theoretical ratio and the measured signal for  $^{29}\text{Si}^{16}\text{O}^+$ ). Fig. 6a shows the calibration graph measured at the maximum of the afterpeak and a high  $y$ -

1  
2  
3 value corresponding to the spectral background is observed. Fig. 6b collects  
4 experimental results by measuring the standards at 0.15 ms after pulse ignition (prepeak  
5 region). In this case, the spectral background was lower while the linear correlation was  
6 improved. However, a small y-value corresponding to the spectral background was  
7 observed corresponding to  $^{12}\text{C}^{16}\text{O}_2^+$  (in any case, the signal for this polyatomic is rather  
8 constant since the correlation of the data are rather good). From the results obtained for  
9 the five glass standards containing calcium, we have selected for quantification studies  
10 the measurement of  $m/z$  44 at the prepeak region.  
11  
12

13  
14  
15  
16  
17  
18 Finally, in order to check the validity of the calibration curves experimentally  
19 obtained, the standard E1 was analysed using the proposed quantification strategy.  
20 Intensities measured for the different analytes in E1 standard were introduced into the  
21 calibration curves and concentrations obtained are collected in Table 2. As can be seen,  
22 experimental results were in good agreement with certified within given uncertainties.  
23  
24  
25  
26  
27

### 28 **3.3. Analysis of the coated glasses**

29  
30 Fig. 7 shows the qualitative depth profiles (signal intensity *versus* sputtering time)  
31 obtained for the investigated glasses coated with thin layers, selecting for each isotope  
32 the previously optimised position in the pulse profile for the data treatment. In the case  
33 of TL1 sample (Fig. 7a), the external  $\text{Si}_x\text{N}_y$  layer and the presence of other elements in  
34 the layer (such as aluminium) are apparent. Moreover, the intermediate Nb layer can be  
35 clearly distinguished. Similarly, Fig. 7b shows the qualitative depth profile obtained for  
36 the more complex TL2 sample. In this case, a very thin external layer of Ti overlapped  
37 with the  $\text{Si}_x\text{N}_y$  layer. Also, the 7 nm thick Cr layer can be observed between the two  
38 non-conductive layers. However, it was not possible to clearly discriminate the thin 20  
39 nm  $\text{SiO}_2$  layer from the  $\text{SiO}_2$  glass substrate in any of the two samples (this could be  
40 attributed to small  $\text{SiO}_2$  concentration differences between both regions and also to the  
41 fact that there is a loss in depth profiling capabilities with the GD for deep layers). On  
42 the other hand, it should be emphasised that the analysis time necessary to measure the  
43 different coating layers was below 1 min, proving once again that rf-PGD-ToFMS  
44 offers an excellent tool for the fast and direct control of coated glasses industrial  
45 production.  
46  
47  
48  
49  
50  
51  
52  
53  
54  
55  
56  
57

58 The qualitative depth profiles, directly obtained by rf-PGD-ToFMS, were used to  
59 calculate the corresponding elemental concentrations making use of the above described  
60 calibration equations (Figs. 5 and 6). Both, the quantitative analysis of the non-

1  
2  
3  
4  
5  
6  
7  
8  
9  
10  
11  
12  
13  
14  
15  
16  
17  
18  
19  
20  
21  
22  
23  
24  
25  
26  
27  
28  
29  
30  
31  
32  
33  
34  
35  
36  
37  
38  
39  
40  
41  
42  
43  
44  
45  
46  
47  
48  
49  
50  
51  
52  
53  
54  
55  
56  
57  
58  
59  
60

conductive layers and the glass substrates were carried out. It should be noted that for the quantification of the conductive layers (e.g. Nb and Cr) conductive standards (described in the Experimental section) were employed to construct the corresponding calibration graphs (not shown in the manuscript). Measured intensity signals for each analyte (e.g. Si) were used to calculate the corresponding element mass content ([Si]) at each position of the depth profile, making use of the calibration equation. Similarly to the calculations with emission yields for GD-OES depth quantification,<sup>14</sup> the absolute sensitive factor of the isotope selected for each element (obtained from the respective calibration curve) and the signal intensity measured for the corresponding isotope are employed to calculate the mass of the element at each position of the depth profile. Next, the “total sputtered mass” in this time interval will be the sum of all the elements present in the sample during this interval. Finally, the concentration of each element during each time interval can be easily calculated as a fraction of the afore mentioned sum. On the other hand, sputtering time can be converted into depth, with the extracted volume in each time interval and taking into account the area analysed (4 mm).

Fig. 8 shows the quantitative depth profiles obtained by rf-PGD-ToFMS for TL1 and TL2 samples. As can be seen, good depth resolution can be observed in both cases for the analysis of thin conductive and non-conductive layers. The thickness of the external layer was regarded as the depth from the beginning of the profile to the point at which the intensity is half of the maximum, and the thickness of the internal layers was regarded as the distance between the two points at which the intensities are half of their maximum. The values observed for layer thickness, obtained as the mean of results from three independent replicates, were:  $23 \pm 2$  nm  $\text{Si}_x\text{N}_y$  and  $9.5 \pm 1$  nm Nb for TL1 sample, and  $3.5 \pm 0.5$  nm Ti,  $8 \pm 1$  nm  $\text{Si}_x\text{N}_y$  and  $5 \pm 0.5$  nm Cr for TL2 sample. The thickness obtained for the external layer was always slightly less than the nominal value, but the measured thickness of the internal layers was in good agreement with the values of the manufacturer (it should be noted that layers thickness on the glasses are not really certified and the RSD of the layer thickness given by the manufacturer was  $\pm 10\%$ ). Additionally, it should be noted that the observed elemental concentrations in the glass substrate were in good agreement with the nominal concentrations of the analysed glass.

Finally, it is interesting also to note that the capabilities of the rf-PGD-ToFMS to provide a full mass spectrum every  $33 \mu\text{s}$  enable the identification of unexpected elements which can be present as contaminants in very thin layers (e.g. Fig. 9

1  
2  
3 demonstrates the presence of impurities of Cd, Sn, Te and Sb within the 20 nm SiO<sub>2</sub>  
4 inner layer of the TL2 sample).  
5  
6  
7

#### 8 9 **4. CONCLUSIONS**

10 Rf-PGD-ToFMS is an analytical technique which can be considered in its infancy.  
11 Analytical methods and applications are then still rather scarce. This work evaluates rf-  
12 PGD-ToFMS performance for the elemental quantitative analysis of glasses and of thin  
13 layers on glasses for the first time and demonstrates that fast analytical characterization  
14 of non conductive samples are at hand.  
15  
16  
17

18 First of all, our results show that although the quantitative aspect could be  
19 improved, it offers a very convenient tool for quantitative analysis of insulators and  
20 layered samples. Moreover, it should be also highlighted the ability of the rf-PGD-  
21 ToFMS for the identification of unexpected elements in thin layers, as demonstrated in  
22 Fig. 9. This work warrants further analytical applications of the technique to tackle real  
23 analytical challenges in the field.  
24  
25  
26  
27  
28  
29  
30

#### 31 **ACKNOWLEDGEMENTS**

32 Financial support from “Plan Nacional de I+D+I” (Spanish Ministry of Science  
33 and Innovation and FEDER Program) through MAT2010-20921-C02 is gratefully  
34 acknowledged. Also, we are particularly thankful to Horiba JobinYvon for the loan of  
35 the GD-ToFMS prototype.  
36  
37  
38  
39  
40  
41  
42  
43  
44  
45  
46  
47  
48  
49  
50  
51  
52  
53  
54  
55  
56  
57  
58  
59  
60

## REFERENCES

- <sup>1</sup> J. Pisonero, N. Bordel, C. González de Vega, B. Fernández, R. Pereiro and Sanz-Medel, Critical evaluation of the potential of radiofrequency pulsed glow discharge-time-of-flight mass spectrometry for depth-profile analysis of innovative materials, *Anal. Bioanal. Chem.*, 2013, **405**, 5655-5662.
- <sup>2</sup> M. R. Winchester and R. Payling, Radio-frequency glow discharge spectrometry: A critical review, *Spectrochim. Acta Part B*, 2004, **59**, 607-666.
- <sup>3</sup> Ph. Belenguer, M. Ganciu, Ph. Guillot and Th. Nelis, Pulsed glow discharges for analytical applications, *Spectrochim. Acta Part B*, 2009, **64**, 623-641.
- <sup>4</sup> M. Voronov, P. Smid, V. Hoffmann, Th. Hofmann and C. Venzago, Microsecond pulsed glow discharge in fast flow Grimm type sources for mass spectrometry, *J. Anal. At. Spectrom.*, 2010, **25**, 511-518.
- <sup>5</sup> R. Pereiro, A. Solà-Vázquez, L. Lobo, J. Pisonero, N. Bordel, J. M. Costa, and A. Sanz-Medel, Present and future of glow discharge - time of flight mass spectrometry in analytical chemistry, *Spectrochim. Acta Part B*, 2011, **66**, 399-412.
- <sup>6</sup> J. A. Klingler, C. M. Barshick and W. W. Harrison, Factors influencing ion signal profiles in pulsed glow discharge mass spectrometry, *Anal. Chem.*, 1991, **63**, 2571-257.
- <sup>7</sup> L. Lobo, J. Pisonero, N. Bordel, R. Pereiro, A. Tempez, P. Chapon, J. Michler, M. Hohl, and Sanz-Medel, A comparison of non-pulsed radiofrequency and pulsed radiofrequency glow discharge orthogonal time-of-flight mass spectrometry for analytical purposes, *J. Anal. At. Spectrom.*, 2009, **24**, 1373-1381.
- <sup>8</sup> J. Pisonero, R. Valledor, A. Licciardello, C. Quirós, J.I. Martín, A. Sanz-Medel and N. Bordel, Pulsed rf-GD-TOFMS for depth profile analysis of ultrathin layers using the analyte prepeak region, *Anal. Bioanal. Chem.*, 2012, **403**, 2437-2448.
- <sup>9</sup> K. G. Reinsberg, C. Schumacher, A. Tempez, K. Nielsch and J.A.C. Broekaert, Depth-profile analysis of thermoelectric layers on Si wafers by pulsed r.f. glow discharge time-of-flight mass spectrometry, *Spectrochimica Acta Part B*, 2012, **76**, 175-180.
- <sup>10</sup> L. Lobo, B. Fernández, R. Pereiro, N. Bordel, E. Demenev, D. Giubertoni, M. Bersani, P. Hönicke, B. Beckhoff and A. Sanz-Medel, Quantitative depth profiling of boron and arsenic ultra-low energy implants by pulsed radiofrequency glow discharge time of flight mass spectrometry, *J. Anal. At. Spectrom.*, 2011, **26**, 542- 549.
- <sup>11</sup> S. Canelescu, I. S. Molchan, C. Tauziède, A. Tempez, J. A. Whitby, G. E. Thompson, P. Skeldon, P. Chapon and J. Michler, Detection of negative ions in glow discharge mass spectrometry for analysis of solid specimens, *Anal. Bioanal. Chem.*, 2010, **396**, 2871-2879.

<sup>12</sup> C. González de Vega, B. Fernández, N. Bordel, R. Pereiro and A. Sanz-Medel, Challenging identifications of polymer coatings by radiofrequency pulsed glow discharge-time of flight mass spectrometry, *J. Anal. At. Spectrom.*, 2013, **28**, 1054-1060.

<sup>13</sup> A.C. Muñoz, J. Pisonero, L. Lobo, C. Gonzalez, N. Bordel, R. Pereiro, A. Tempez, P. Chapon, N. Tucitto, A. Licciardello and A. Sanz-Medel, Pulsed radiofrequency glow discharge time of flight mass spectrometer for the direct analysis of bulk and thin coated glasses, *J. Anal. At. Spectrom.*, 2008, **23**, 1239-1246.

<sup>14</sup> Glow Discharge Optical Emission Spectroscopy: A Practical Guide, Th. Nelis and R. Payling, The Royal Society of Chemistry, UK, 2003.

<sup>15</sup> M. Vázquez Peláez, J. M. Costa-Fernández, R. Pereiro, N. Bordel and A. Sanz-Medel, Quantitative depth profile analysis by direct current glow discharge time of flight mass spectrometry, *J. Anal. At. Spectrom.*, 2003, **18**, 864-871.

<sup>16</sup> S. Mushtaq, V. Hoffmann, E. B. M. Steers and J. C. Pickering, Comparison of a sample containing oxide with a pure sample with argon–oxygen mixtures, *J. Anal. At. Spectrom.*, 2012, **27**, 1423-1431.

<sup>17</sup> M. Hohl, A. Kanzari, J. Michler, T. Nelis, K. Fuhrer and M. Gonin, Pulsed r.f.-glow-discharge time-of-flight mass spectrometry for fast surface and interface analysis of conductive and non-conductive materials, *Surf. Interf. Anal.*, 2006, **38**(4), 292-295.

<sup>18</sup> M. Bouza, B. Fernandez, C. Gonzalez-Gago, N. Bordel, R. Pereiro and A. Sanz-Medel, Rf-pulsed glow discharge time-of-flight mass spectrometry for glass analysis: investigation of the ion source design, *Anal. Chim. Acta*, 2012, **756**, 30-36.

<sup>19</sup> J. H. Barnes IV, O. A. Gron, and G. M. Hieftje, Determination of Ca<sup>+</sup> and K<sup>+</sup> by pulsed glow discharge sector-field mass spectrometry, *J. Anal. At. Spectrom.*, 2004, **19**, 1564-1566.

<sup>20</sup> C. L. Lewis, E. S. Oxley, C. K. Pan, R. E. Steiner and F. L. King, Determination of <sup>40</sup>Ca<sup>+</sup> in the presence of <sup>40</sup>Ar<sup>+</sup>: An illustration of the utility of time-gated detection in pulsed glow discharge mass spectrometry, *Anal. Chem.*, 1999, **71**, 230-234.

---

## FIGURE CAPTIONS

**Figure 1.** Afterglow pulse profiles obtained for  $^{23}\text{Na}^+$ ,  $^{24}\text{Mg}^+$ ,  $^{27}\text{Al}^+$ ,  $^{28}\text{Si}^+$  and  $m/z$  40 measured by rf-GD-ToFMS using D1 material. The GD selected experimental conditions were 300 Pa and 80 W.

**Figure 2.** a) Mass spectra for  $^{48}\text{Ti}^+$  obtained for JK-41-N CRM (25% Ti, 6.9% N). In the legend of the figure “Maximum” means that the measurement has been made at the maximum position of the afterglow, “complete” that the whole afterglow was used for measurement, “beginning” at the earlier part of the afterglow, “final” at the latter part of the afterglow, and “2.25-2.4 ms” that the pulse interval between 2.25 ms and 2.4 ms after starting the corresponding GD cycle was measured; b) Evaluation of the mass spectra of silicon isotopes ( $m/z$  28, 29 and 30) collected at the pulse profile region between 2.25-2.4 ms for three different samples with variable  $\text{SiO}_2$  contain.

**Figure 3.** Pulse profiles obtained under the selected experimental conditions (300 Pa and 80W) for  $^{38}\text{Ar}^1\text{H}^+$  polyatomic ion analysing the standard B1 and for  $^{36}\text{Ar}^1\text{H}^+$  and  $m/z$  39 analysing the standard F1 (19.3%  $\text{K}_2\text{O}$ ). The dashed rectangle indicates the time region where the analytical measurements are carried out.

**Figure 4.** Mass spectra obtained at the prepeak region for the analysis of three standards: NIST 621 glass (10.7% Ca, 72.13% Si), NIST 93A glass (0.01% Ca, 80.8% Si) and 151X-FCA4 stainless steel (0% Ca, 0.01% Si). a)  $m/z$  44, b)  $m/z$  45

**Figure 5.** Calibration graphs obtained for  $^{27}\text{Al}^+$ ,  $^{16}\text{O}^+$ ,  $^{28}\text{Si}^+$ ,  $^{39}\text{K}^+$  and  $^{23}\text{Na}^+$  by rf-PGD-ToFMS using the glass calibration standards collected in Table 1 (except E1) and employing the GD selected experimental conditions (300 Pa and 80 W). The GD pulse time window selected has been the interval 2.25-2.4 ms after pulse ignition for all isotopes excepting  $^{39}\text{K}^+$  (33  $\mu\text{s}$  interval at 2.7 ms after the pulse ignition was selected in this case).

1  
2  
3  
4  
5  
6  
7  
8 **Figure 6.** Calibration graphs obtained for calcium. a)  $m/z$  44 measuring at the afterpeak  
9 maximum, b)  $m/z$  44 measuring at 0.15 ms after pulse ignition (prepeak region).  
10  
11

12  
13 **Figure 7.** Qualitative depth profiles obtained by rf-PGD-ToFMS under the selected  
14 experimental conditions. a) TL1 sample, b) TL2 sample.  
15  
16

17  
18 **Figure 8.** Quantitative depth profiles obtained by rf-PGD-ToFMS under the selected  
19 experimental conditions. A) 27 nm  $\text{Si}_x\text{N}_y$ /12 nm Nb/20 nm  $\text{SiO}_2$ //6 mm glass (TL1) and  
20 4 nm Ti/10 nm  $\text{Si}_x\text{N}_y$ /6 nm Cr/20 nm  $\text{SiO}_2$ //6 mm glass (TL2).  
21  
22  
23  
24

25  
26 **Figure 9.** Mass spectra obtained within the 20 nm  $\text{SiO}_2$  inner layer of TL2 sample. a)  
27  $m/z$  interval: 107 - 121, b)  $m/z$  interval: 120 - 130.  
28  
29  
30  
31  
32  
33  
34  
35  
36  
37  
38  
39  
40  
41  
42  
43  
44  
45  
46  
47  
48  
49  
50  
51  
52  
53  
54  
55  
56  
57  
58  
59  
60

Figure 1

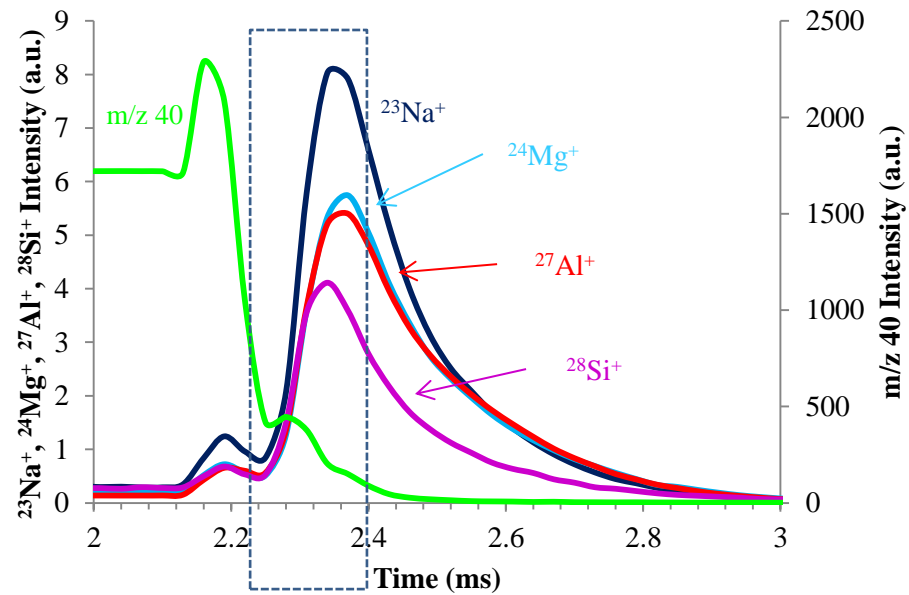


Figure 2

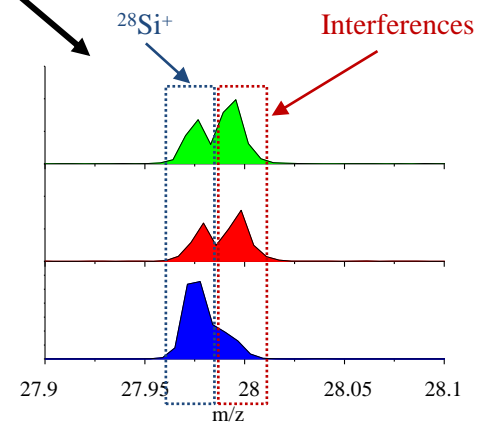
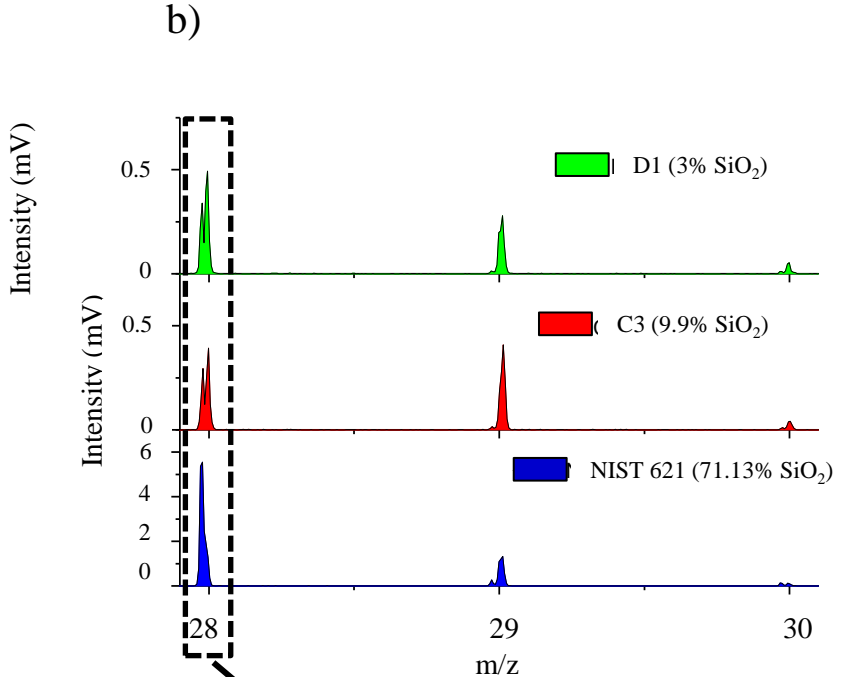
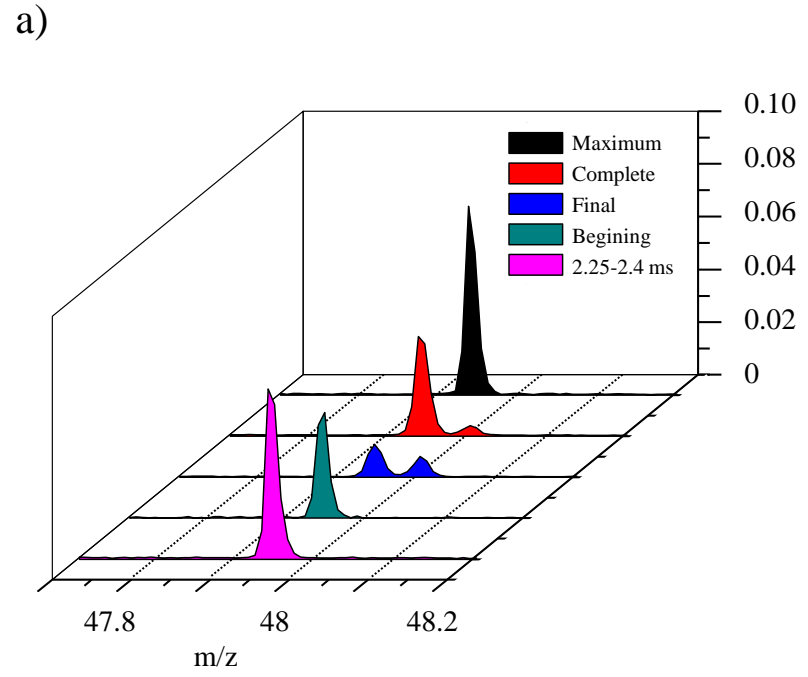


Figure 3

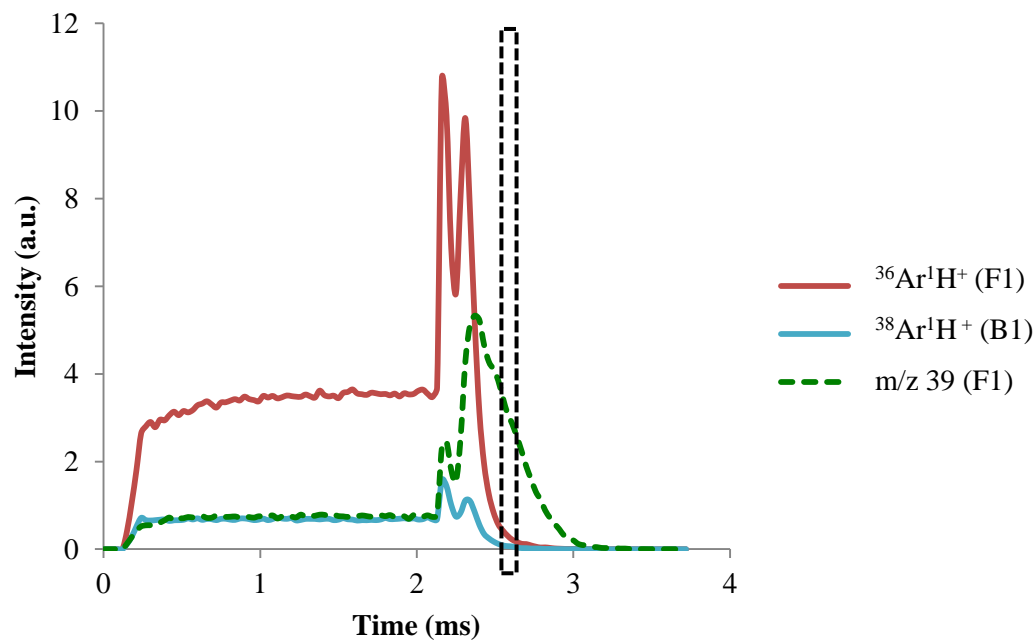
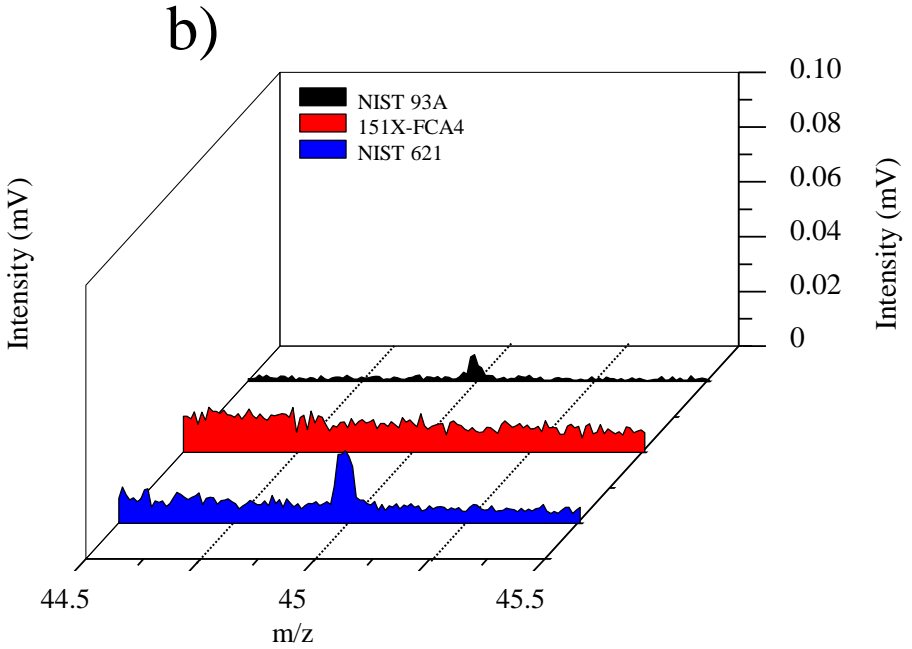
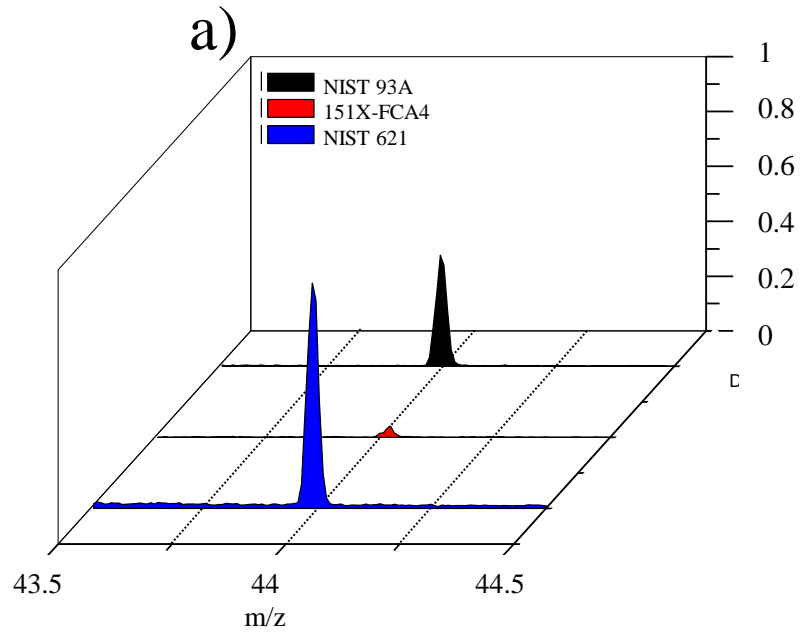


Figure 4



1  
2  
3  
4  
5  
6  
7  
8  
9  
10  
11  
12  
13  
14  
15  
16  
17  
18  
19  
20  
21  
22  
23  
24  
25  
26  
27  
28  
29  
30  
31  
32  
33  
34  
35  
36  
37  
38  
39  
40  
41  
42  
43

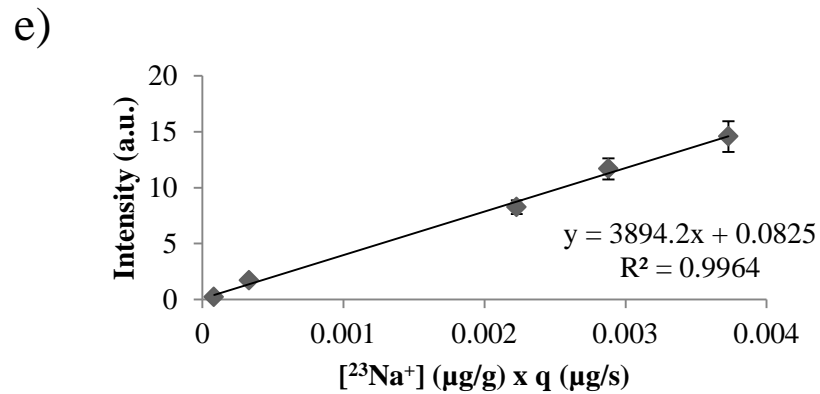
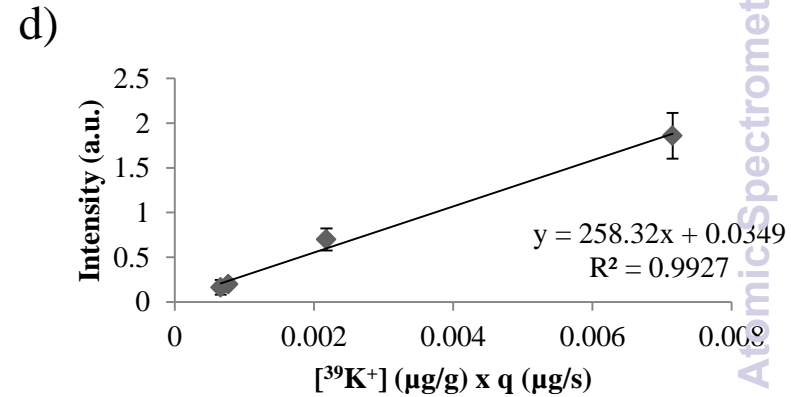
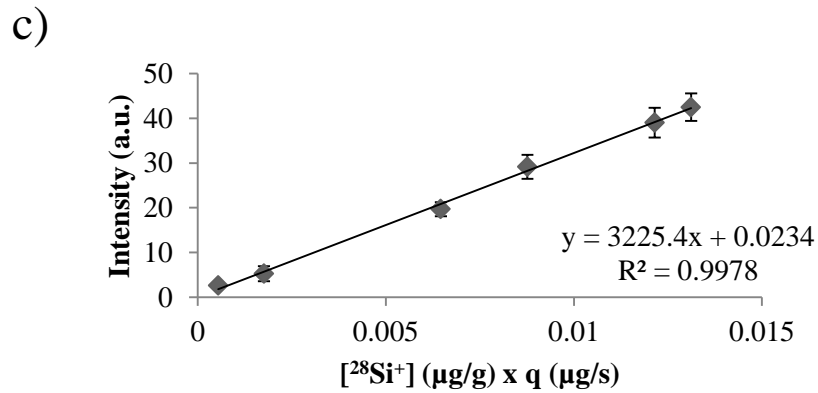
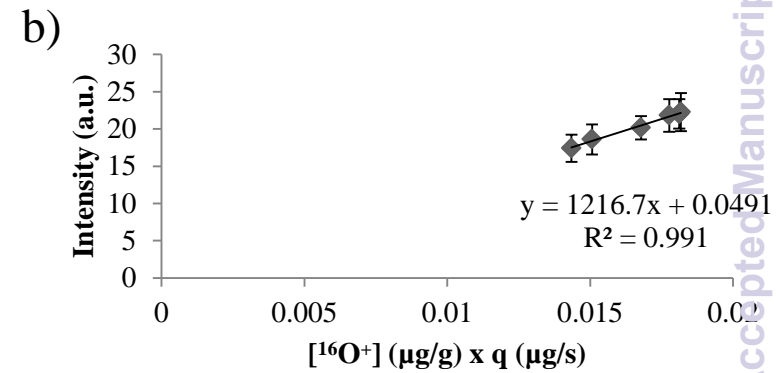
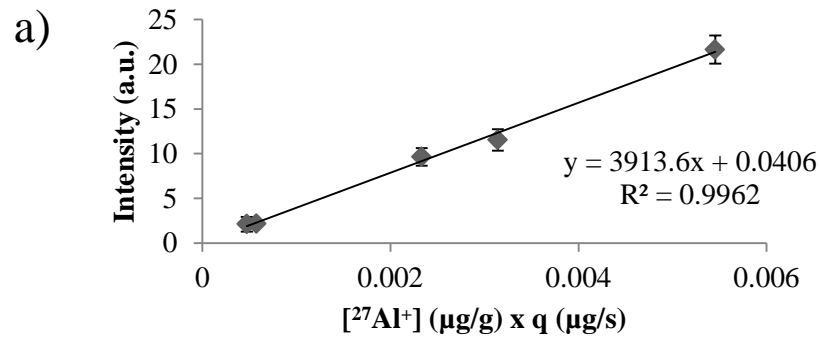
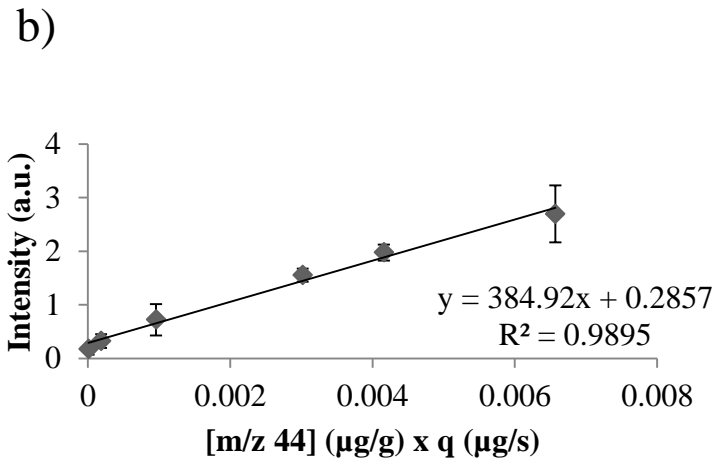
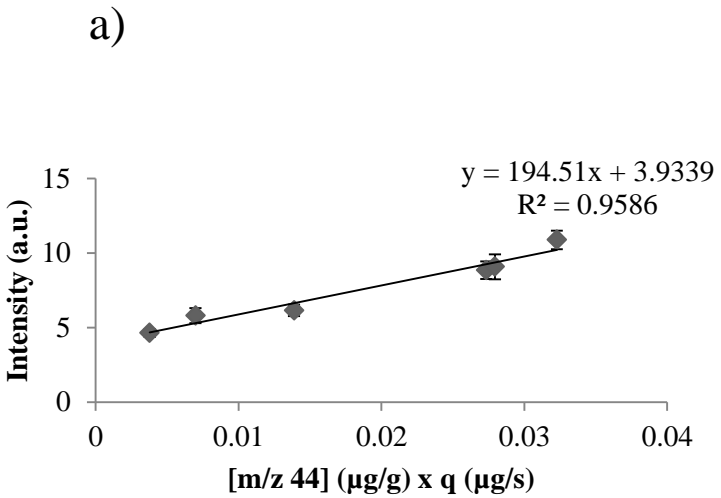


Figure 5

Figure 6



1  
2  
3  
4  
5  
6  
7  
8  
9  
10  
11  
12  
13  
14  
15  
16  
17  
18  
19  
20  
21  
22  
23  
24  
25  
26  
27  
28  
29  
30  
31  
32  
33  
34  
35  
36  
37  
38  
39  
40  
41  
42  
43

Figure 7

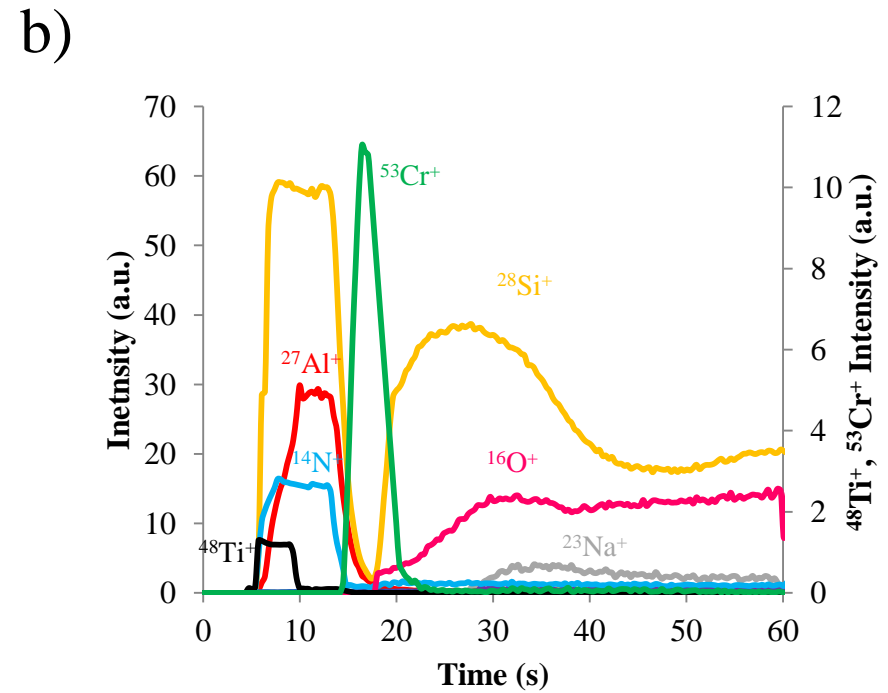
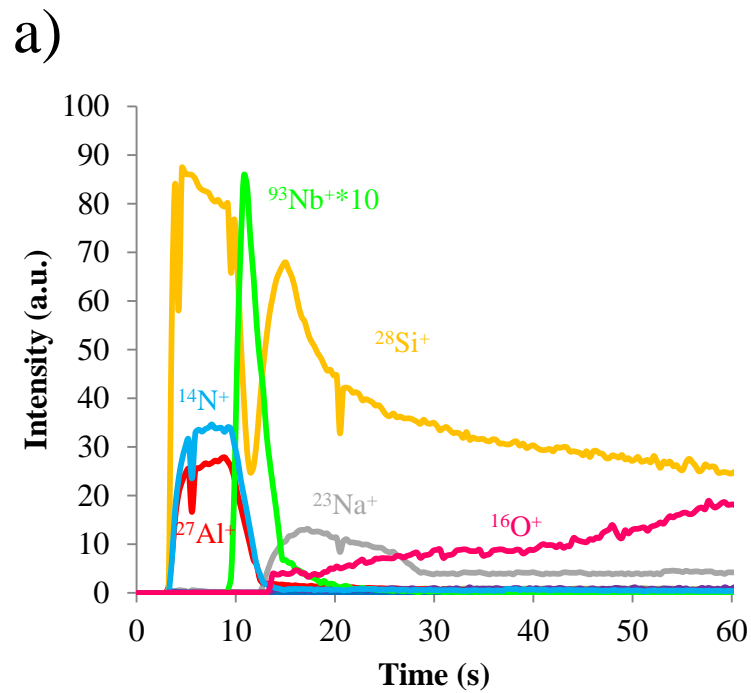


Figure 8

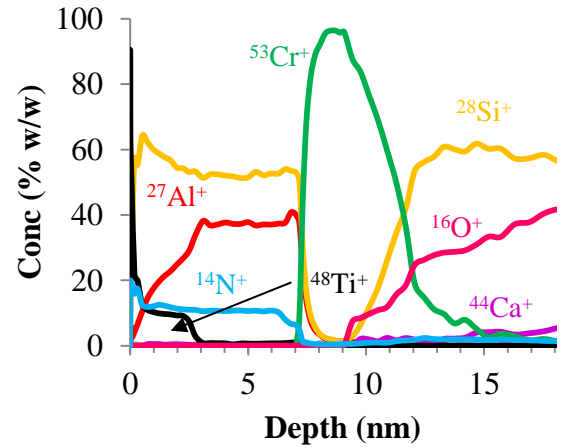
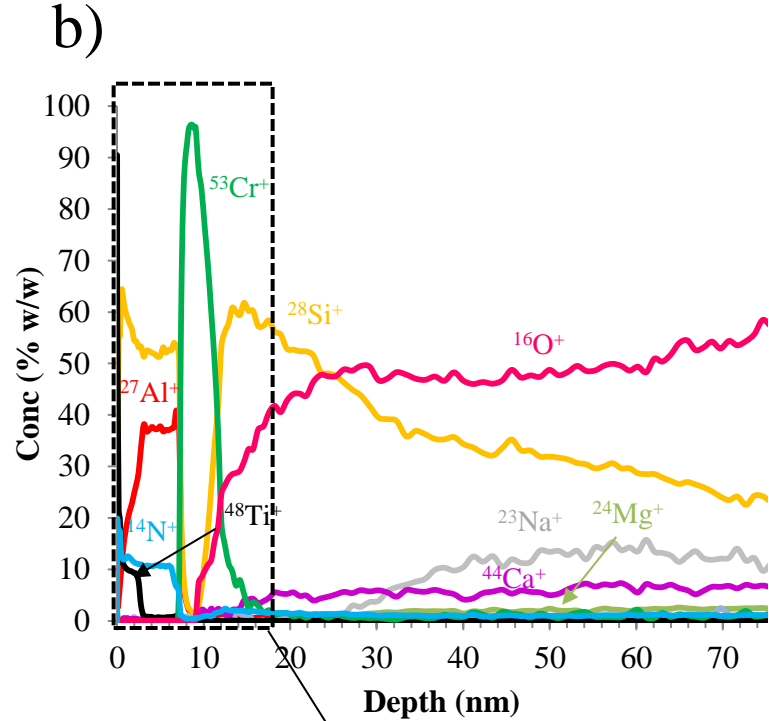
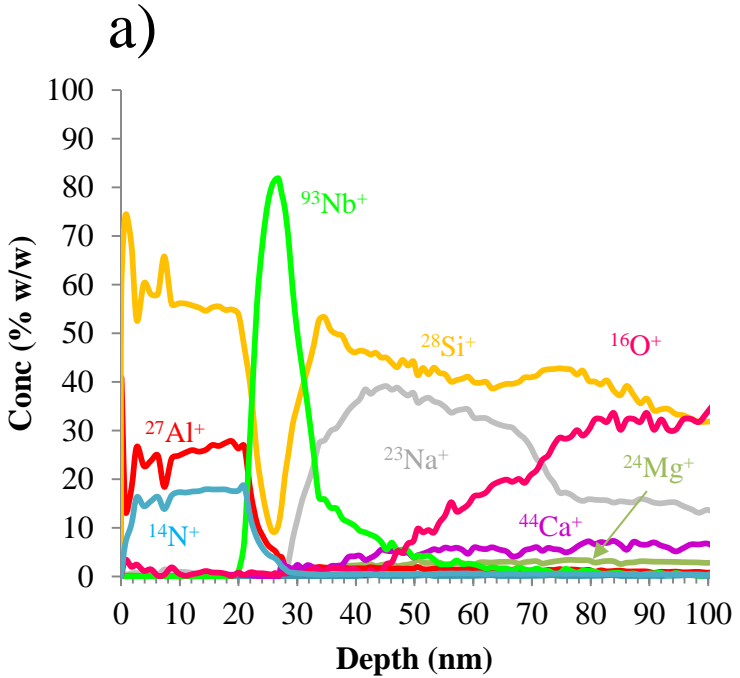
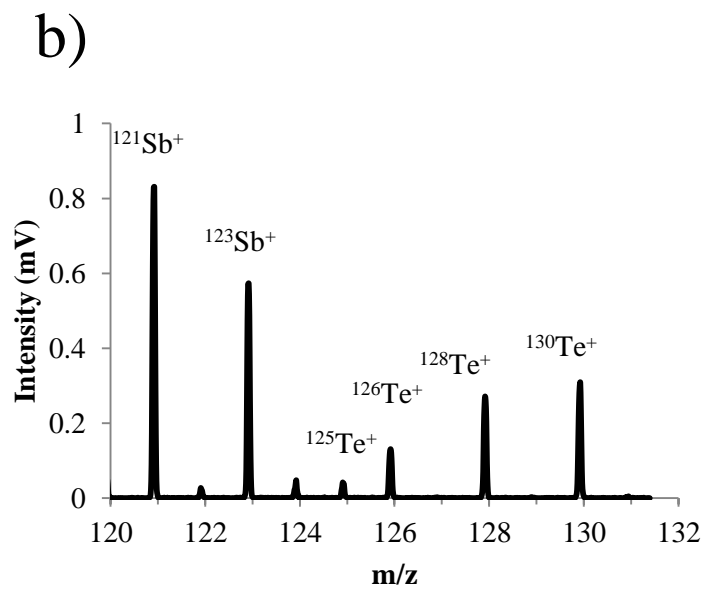
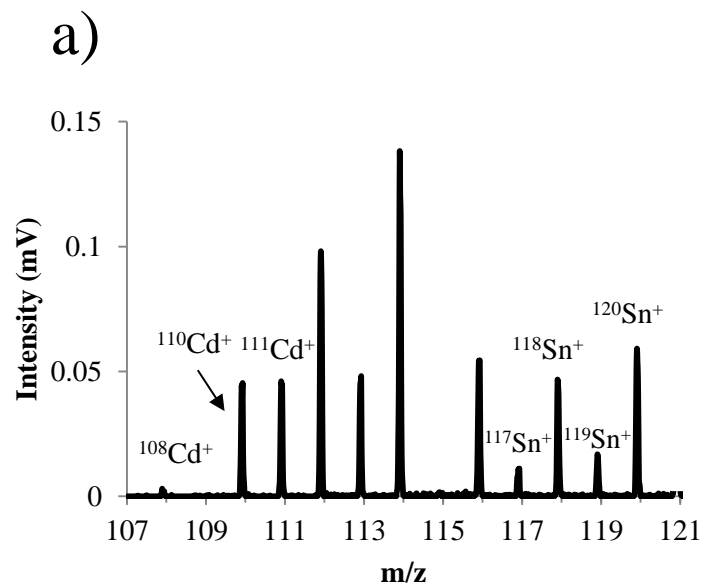


Figure 9



**Table 1.** Chemical composition (in % w/w) and sputtering rate ( $\mu\text{g s}^{-1}$ ) of non conductive calibration standards.

Standard	SiO <sub>2</sub> (%)	Na <sub>2</sub> O (%)	MgO (%)	Al <sub>2</sub> O <sub>3</sub> (%)	K <sub>2</sub> O (%)	CaO (%)	q <sub>m</sub> ( $\mu\text{g s}^{-1}$ )
<b>NIST 621</b>	71.13	12.74	0.27	2.76	2.01	10.71	0.050±0.004
<b>F1</b>	58.23	1	1	2	19.3	3	0.044±0.002
<b>B1</b>	51					25	0.037±0.003
<b>E1</b>	50.9	15		1.5	2.5	5	--
<b>A2</b>	36.8	0.3	3.5	12	2.5	0.7	0.037±0.002
<b>C3</b>	9.9	7.9		27.1		0.03	0.038±0.003
<b>D1</b>	3	10	9	15.3	6.9	15	0.039±0.003

**Table 2.** Determination of Na, Al, Si, K and Ca mass fraction (as oxides in % w/w) in standard E1 by rf-PGD-ToFMS. Uncertainty is expressed as the standard deviation of n = 3 independent analyses.

<b>E1</b>	<b>Na<sub>2</sub>O (%)</b>	<b>Al<sub>2</sub>O<sub>3</sub> (%)</b>	<b>SiO<sub>2</sub> (%)</b>	<b>K<sub>2</sub>O (%)</b>	<b>CaO (%)</b>
<b>Certified Concentration</b>	15	1.5	50.9	2.5	5
<b>rf-PGD-ToFMS Concentration</b>	14.1±1.5	1.7±0.3	49.4±2.7	2.4±0.3	4.6±1.1